

Supplementary Information :

A point-of-care microfluidic channel-based device for the rapid and direct detection of fibrinogen in whole blood

Qinan Ban^{1,2,#}, Yulong Zhang^{1#}, Yuxuan Li¹, Daye Cao³, Weifeng Ye⁴, Linsheng

Zhan^{1,2,}, Daming Wang^{3,5*}, Xiaohui Wang^{1,*}*

1: Institute of Health Service and Transfusion Medicine, Beijing 100850, P. R. China

2: BGI college, Zhengzhou University, Henan, 450001, P. R. China

3: Anbio (Xiamen) Biotechnology Co., Ltd, Xiamen, Fujian Province, 361028, P. R. China

4: Center of Clinical Laboratory, Beijing Friendship Hospital, Capital Medical University, Beijing 100050, P. R. China

5: Suzhou Institute of Biomedical Engineering and Technology (SIBET), Chinese Academy of Sciences. Suzhou, Jiangsu Province, 215163, P. R. China

#: These authors contributed equally to this work.

*To whom correspondence should be addressed.

Tel.: +86-010-66931049

Fax: +86-010-66931049-

E-mail: lovechina1980@163.com, wangdm@sibet.ac.cn; amms91@126.com

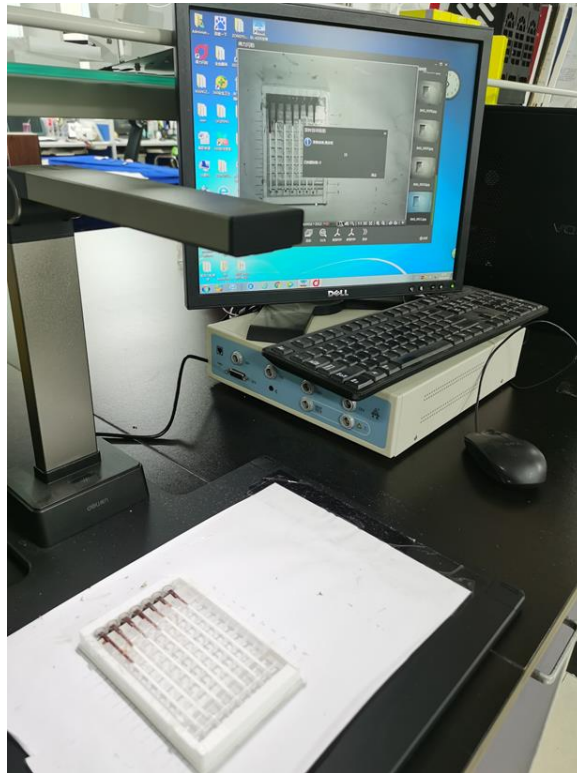


Figure S1. The photographic equipment used during the experiment. Using the HD scanner as a camera device, it can fix the photo height and connect to a computer to synchronize the picture in the computer display screen. The automatic photo time, photo clarity can be controlled by the computer, and the data is finally collected and processed through the computer.

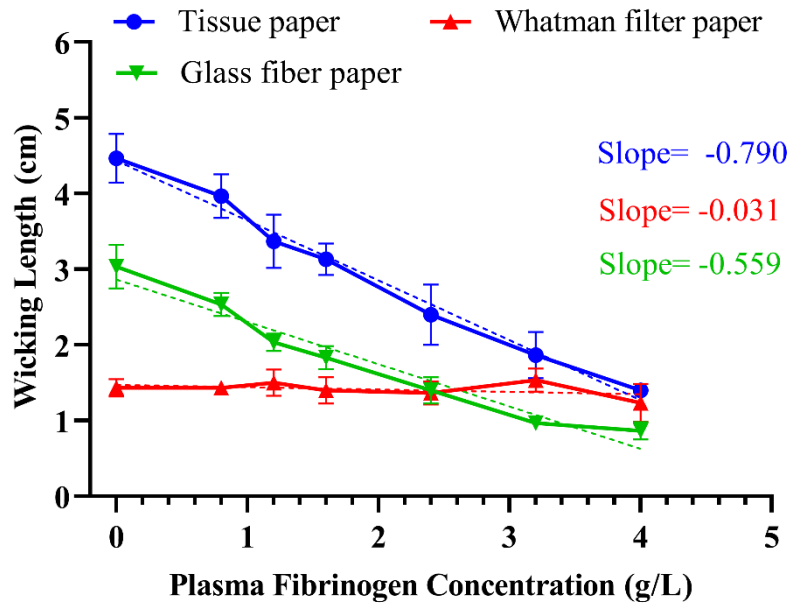


Figure S2. The detection results under different wicking paper types, including Tissue paper, Filter paper, and Glass fiber paper. Each data point was tested 3 times in parallel. After linear fitting of the results in different paper type groups, the slope was given in the right.

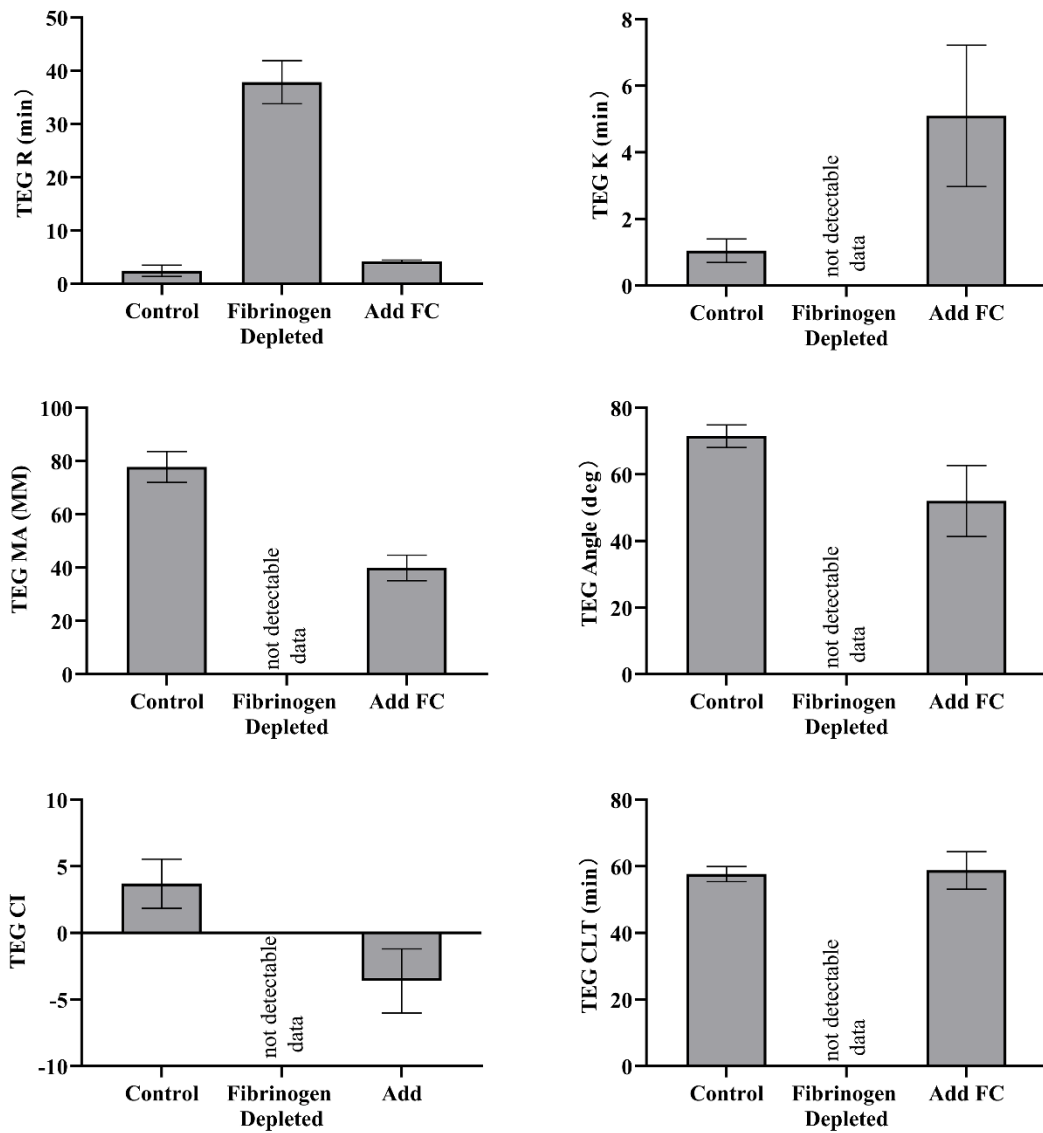


Figure S3. Thromboelastogram data. Compare changes in thromboelastograms between normal whole blood, whole blood after fibrinogen removal, and whole blood with manual fibrinogen addition after removal. After removal of fibrinogen, the blood coagulation function completely disappears, and after the addition of fibrinogen, the coagulation function is gradually restored. Each data point was tested 3 times in parallel.

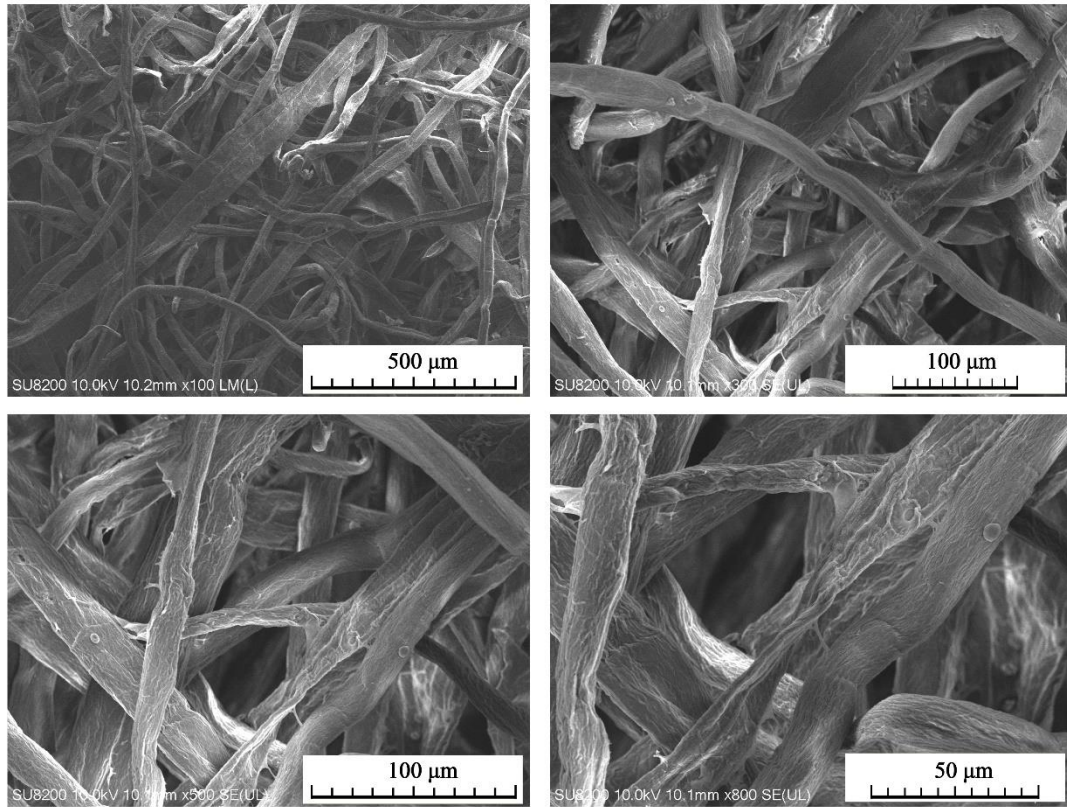


Figure S4. Untreated paper under scanning electron microscopy in fiber structure. The paper has a large pore size and a rough fiber surface, allowing individual red blood cells to pass through, but the blood clot formed by fibrin-encapsulated red blood cells cannot pass through and cross-links with the fibers to cause wick suction blockage.



Figure S5. Comparison of the wicking length of the whole blood samples of four different fibrinogen concentrations on test strips. It can be seen from the figure that the fibrinogen concentrations have significant influence on the wicking lengths.

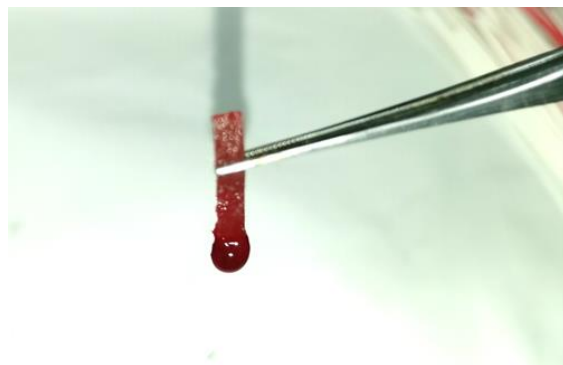


Figure S6. After the wicking completed, the blood clot is schematically presented at the bottom of the reaction strip.

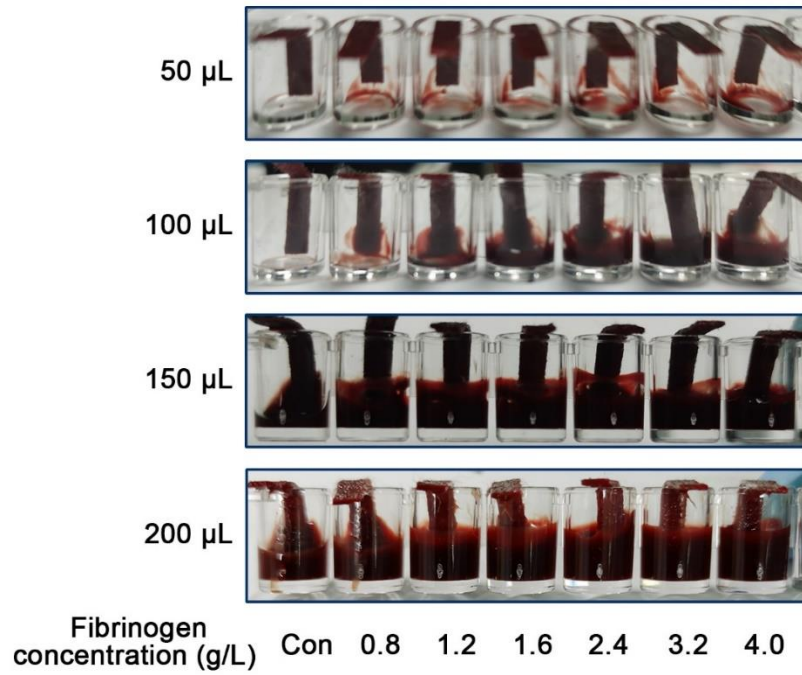


Figure S7. The amount of whole blood remaining in the sample wells after 30s wicking time.

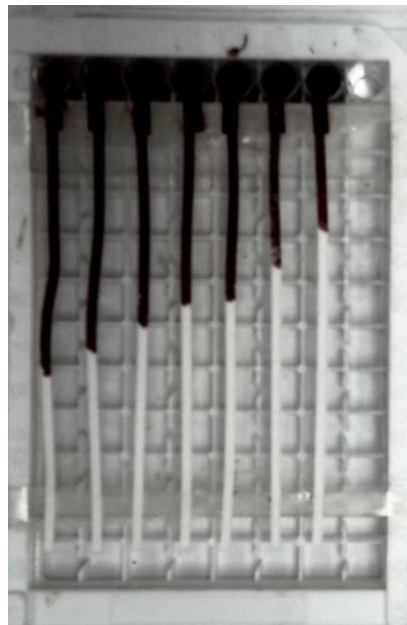


Figure S8. Results obtained under the optimal condition. The fibrinogen concentration has a good linear relationship with the wicking length.

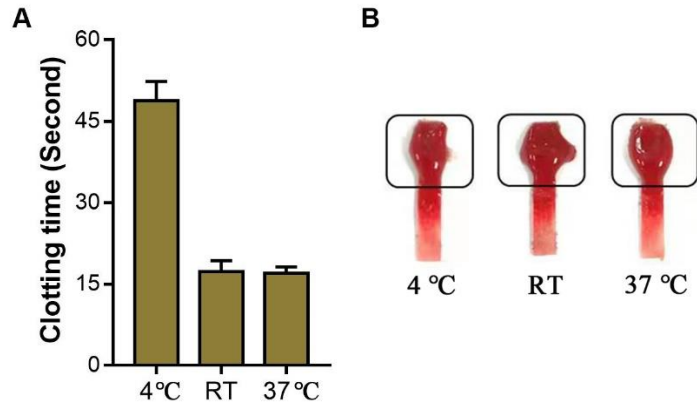


Figure S9. Clotting time (A) and clotting formation on reaction strips (B) under different temperatures. Each data point was tested 3 times in parallel.

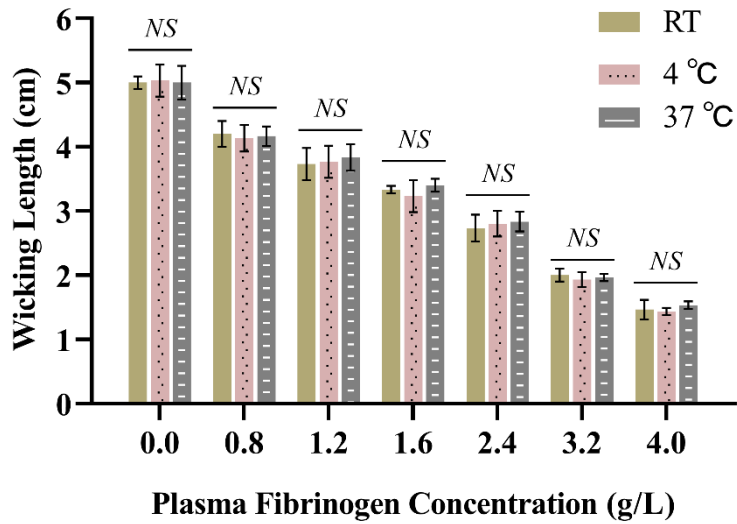


Figure S10. Feasibility test under different temperatures. Each data point was tested 3 times in parallel and presented as Mean±SD. NS represented that there was no significant difference. Two-way ANOVA was employed for the statistical analysis.



Figure S11. POCT devices are designed and manufactured according to the above methods. It made the operation and reading easier and would not affected by external environments.

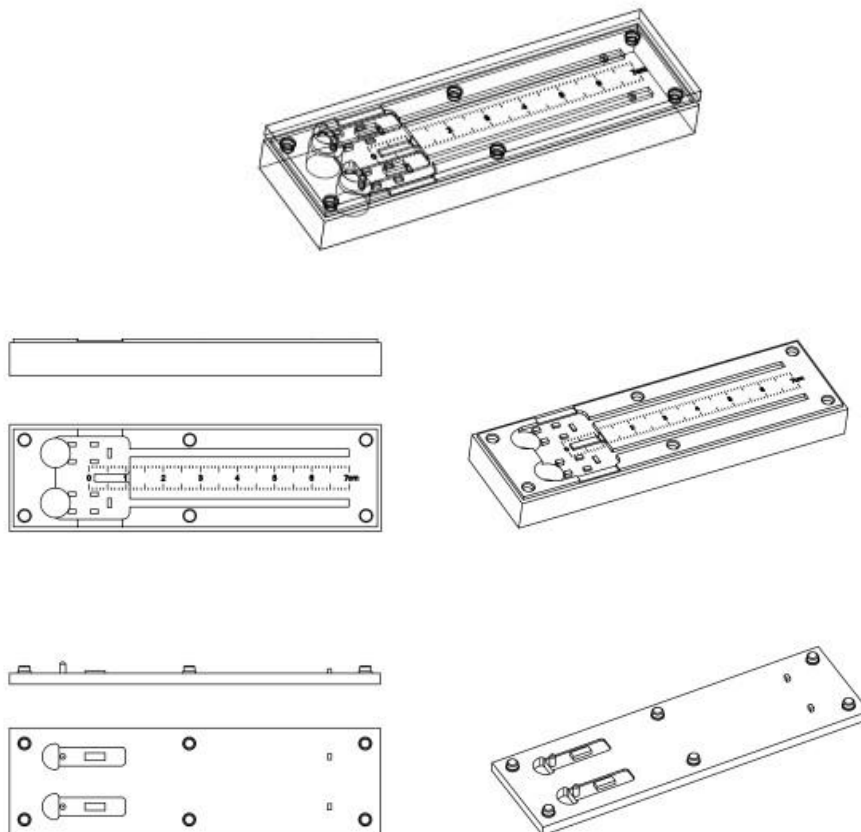


Figure S12. Three views of POCT device structure after optimization.

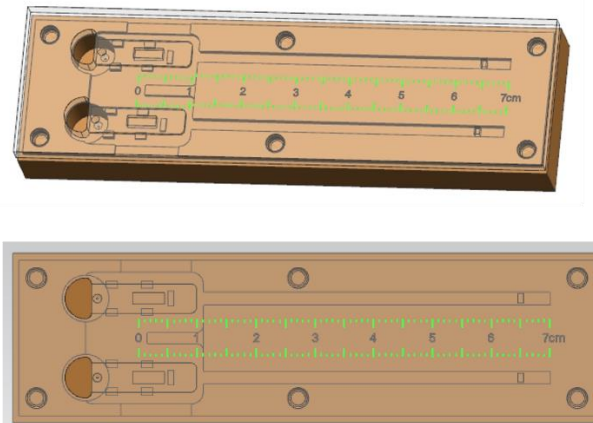


Figure S13. The final POCT device model.

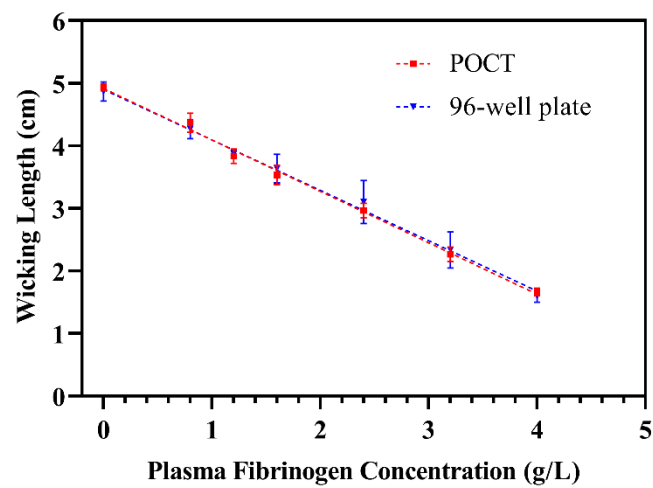


Figure S14. The results obtained in POCT devices are compared with those obtained in 96-well plates. Each data point was tested 3 times in parallel. Their results are consistent well.

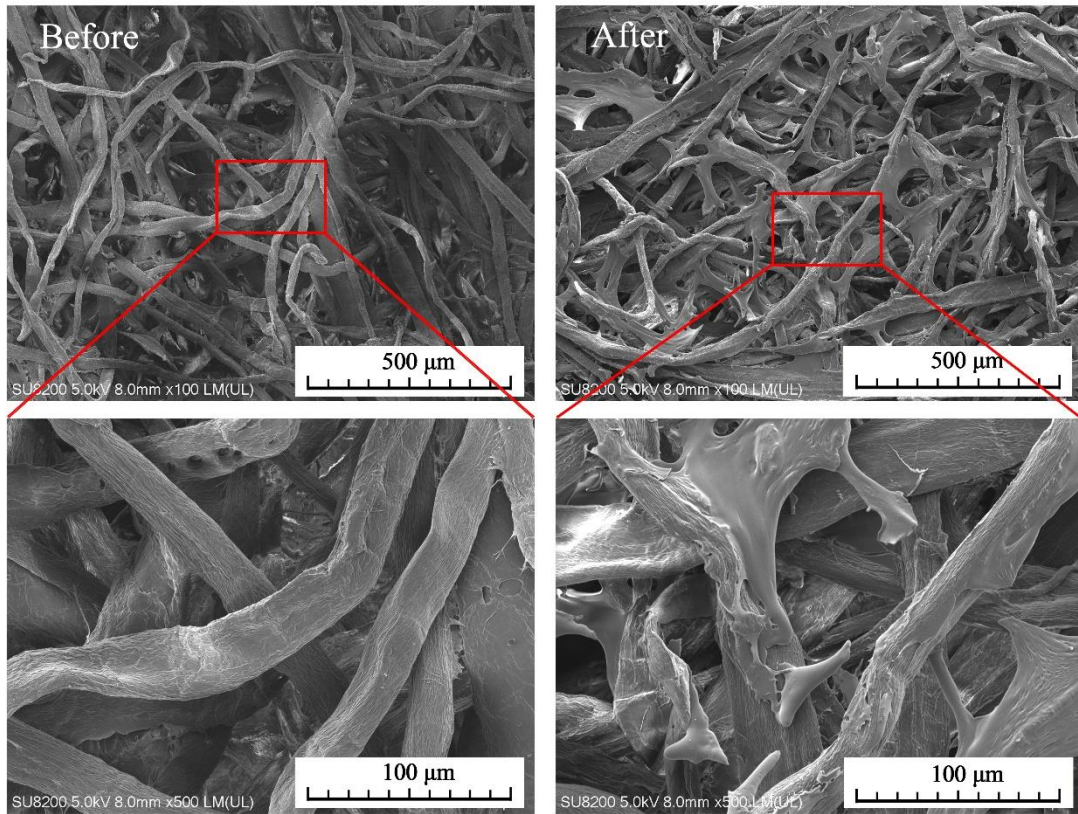


Figure S15. The SEM micrographs of the reaction strip before and after thrombin freeze-drying.

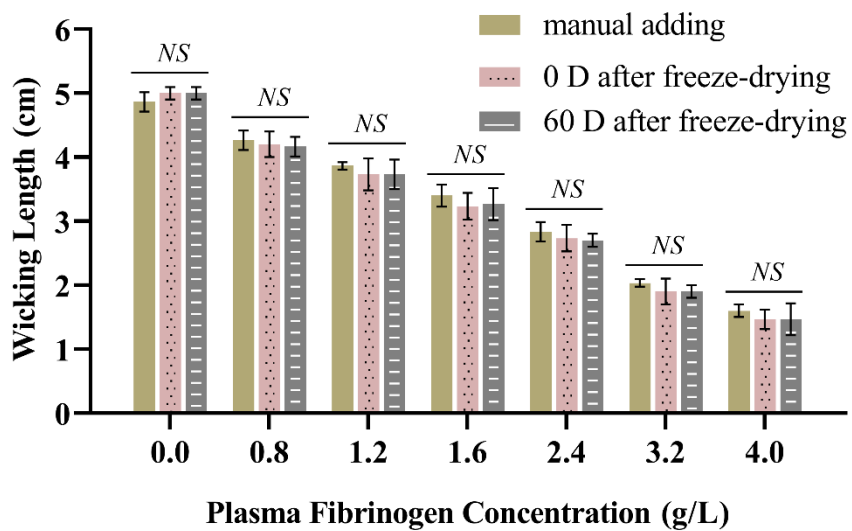


Figure S16. Monitoring thrombin activity after freeze-drying. Each data point was tested 3 times in parallel.

Table S1. Paper types and parameters in paper screening experiment.

Paper type	Cat. No.	Thickness (mm)	Gsm (g/m²)
Tissue paper	347	0.54	103
Filter paper	1003-320	0.39	185
Glass fiber paper	RB65	0.26	53

Table S2. Thrombin freeze-drying process and temperature control process.

Step	Shelf Temperature (°C)	Ramp time (min)	Hold time (min)	Vacuum pressure (Pa)
1	+4.0	0	10	0.0
2	-50.0	0	60	0.0
3	-30.0	0	60	0.0
4	-45.0	0	120	0.0
5	-45.0	0	360	12.0
6	-30.0	60	360	8.0
7	-20.0	30	60	5.0
8	-10.0	10	30	5.0
9	+0.0	10	30	5.0
10	+10.0	10	30	3.0
11	+0.0	20	40	5.0
12	+10.0	20	40	3.0
13	+25.0	10	30	3.0
14	+25.0	10	30	3.0
15	+25.0	10	60	2.0
16	+25.0	10	240	0.0